



A Comparative Analysis of Space Vector Modulation Based Common Mode Voltage Reduction Strategies in a Modular Multilevel Converter

Downloaded from: <https://research.chalmers.se>, 2025-01-15 12:28 UTC

Citation for the original published paper (version of record):

Tang, C., Zhao, J., Thiringer, T. (2024). A Comparative Analysis of Space Vector Modulation Based Common Mode Voltage Reduction Strategies in a Modular Multilevel Converter. *IEEE Access*, 12: 192721-192730.
<http://dx.doi.org/10.1109/ACCESS.2024.3519518>

N.B. When citing this work, cite the original published paper.

© 2024 IEEE. Personal use of this material is permitted. Permission from IEEE must be obtained for all other uses, in any current or future media, including reprinting/republishing this material for advertising or promotional purposes, or reuse of any copyrighted component of this work in other works.

Received 20 November 2024, accepted 10 December 2024, date of publication 18 December 2024,
date of current version 27 December 2024.

Digital Object Identifier 10.1109/ACCESS.2024.3519518

RESEARCH ARTICLE

A Comparative Analysis of Space Vector Modulation-Based Common Mode Voltage Reduction Strategies in a Modular Multilevel Converter

CHENGJUN TANG, (Graduate Student Member, IEEE), JIAN ZHAO ,
AND TORBJÖRN THIRINGER , (Senior Member, IEEE)

Department of Electrical Engineering, Chalmers University of Technology, 412 96 Gothenburg, Sweden

Corresponding author: Jian Zhao (zjian@chalmers.se)

This work was supported by the Area of Advance of Chalmers University of Technology, Swedish Energy Agency under Grant 2017-008071/44949-1.

ABSTRACT In various variable speed applications with power converters, failures in the bearings caused by common mode voltage (CMV) have been frequently reported. This study investigates space vector modulation (SVM)-based strategies for reducing CMV in a modular multilevel converter (MMC). Two strategies for CMV reduction, complete and partial, are examined. The study compares the impact of these strategies on feasibility, total losses, and current total harmonic distortion (THD). Both simulation and experimental results are analyzed, with experiments conducted on a wind turbine emulator driven by a five-level MMC. The findings demonstrate that both strategies can effectively limit CMV amplitude compared to cases without any CMV reduction strategy. The partial CMV reduction strategy, while resulting in a 6.7% increase in switching loss, offers the lowest current THD (0.73%). The complete CMV reduction strategy achieves near-zero CMV and reduces switching loss by 3.9%, but at the cost of the highest current THD (1.81%) and limited DC-link voltage utilization. Experimental results confirm the significant impact of CMV on main bearing performance, as both CMV reduction strategies can reduce the bearing current amplitude and the number of bearing current events. Specifically, the partial CMV reduction strategy extends the bearing lifetime by a factor of 49, while the complete CMV reduction strategy extends it by a factor of 416, both relative to no CMV reduction. These results underscore the effectiveness of CMV reduction strategies in mitigating bearing currents in modern power electronics-based electric drives.


INDEX TERMS Bearing current, common mode voltage, modular multilevel converter, space vector modulation, wind turbine.

I. INTRODUCTION

Electrical machines, which build the bridge between electrical power and mechanical power, are widely used in various drive systems and power generation systems. With the adoption of power electronics, electrical machines can be driven at variable speeds and achieve more flexible arrangements in these systems [1]. As a result, the installation

of electrical machines has increased significantly in recent decades [2], [3], [4], [5].

However, the power electronics controlled by pulse-width modulation (PWM) technology used in variable speed drives also introduce issues for electrical machines. Among these issues, bearing current is a primary concern that reduces the lifespan of electrical machines [6], [7], [8]. One industry sector where bearing current brings problems is the wind power industry. Bearing failures caused by bearing current persist as a prevalent issue in wind turbines, accounting for a significant portion of failures [9], [10], [11].

The associate editor coordinating the review of this manuscript and approving it for publication was Suman Maiti .

It has been noted that high-frequency common mode voltage (CMV) from the converter and electrical machine stray capacitance are critical causes of bearing currents [12], [13], [14]. Studies indicate that a bearing current density (J_b) greater than 0.7 A/mm^2 is harmful to the bearing [15], [16], [17], [18]. Therefore, understanding the mechanism of CMV and finding mitigation methods to achieve low CMV amplitude and thus reduce the bearing current density is of great interest.

To suppress bearing currents, various methods have been studied, including common mode filters, conductive bearing grease, and rotor flange insulation [19], [20], [21]. While effective, these methods often introduce additional components or costs to the system. An alternative approach to suppress bearing currents without adding extra components is to limit the CMV amplitude at the modulation stage when controlling the power electronics converter. In applications utilizing multilevel converters, this approach is highly advantageous due to the flexibility it provides in designing switching schemes that can achieve lower CMV amplitude [22], [23], [24]. Zhang et al. proposed a multilevel converter modulation scheme in [22] that eliminates CMV, specifically for a three-level neutral-point-clamped (NPC) converter. However, in medium voltage applications where higher voltage levels are required, a three-level converter may not be sufficient, and the NPC topology may suffer from unbalanced losses. Edpuganti et al. introduced a CMV elimination scheme using a dual n-level modular multilevel converter (MMC) topology with an open-end stator winding induction motor. However, the dual MMC requirements in the scheme add complexity to the system, and it is not applicable for general applications where only one MMC is utilized [23]. Park et al. studied different CMV reduction strategies in a single MMC setup, including the combined nearest level modulation (NLM) and PWM method to achieve CMV reduction. This method is unfortunately complex, and the actual impact of reduced CMV on bearing current was neither presented nor verified [24].

In this study, MMC has been selected as the converter topology due to its simple structure and high efficiency [25], and the objective of this study is to explore innovative Space Vector Modulation (SVM)-based common mode voltage reduction (CMVR) strategies. The main contribution of this study is the performance quantification of different CMVR mitigation strategies and the experimental verification thereof. Within this scope, one important contribution is a proposal of CMVR strategies based on a generalized SVM scheme, which can be effectively applied to an n -level MMC, addressing the industry’s need for scalable and adaptable solutions. Furthermore, an additional important contribution is a detailed comparison and analysis of losses and total harmonic distortion (THD) between different CMVR strategies in the simulation section. Finally, the practical experimental verification of the effectiveness of different CMVR strategies through measuring the bearing current in a wind turbine emulator, highlighting the

direct implications and benefits for the renewable energy sector.

II. COMMON MODE VOLTAGE AND ITS IMPACT ON THE ELECTRIC MACHINE

The converter output voltage applied on the winding of the electrical machine contains differential mode voltage and common mode voltage. The differential mode voltage appears over the phase windings; however, the common mode voltage is the same over all the phase windings, and it also appears on the middle point of the electrical machine. The general expression for the CMV in the studied application is

$$V_{cm} = \frac{1}{3}(V_{ao} + V_{bo} + V_{co}) \quad (1)$$

where V_{ao} , V_{bo} , and V_{co} are the phase voltages with respect to the middle point of the DC-link of the converter.

The CMV on the winding attempts to find its way to the ground via different paths inside the electrical machine. The structure of the electrical machine is shown in Fig. 1. The equivalent capacitances between different components are illustrated in Fig. 1 as well.

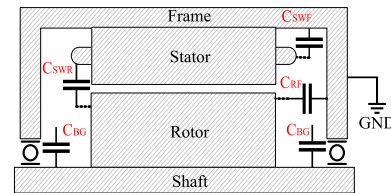


FIGURE 1. Electrical machine structure and capacitance between different components.

The frame of the electrical machine is its ground point. In general, there are two main paths for the CMV to be coupled to the ground point,

- Path A: Stator winding → slot insulation → stator core → machine frame;
- Path B: Stator winding → rotor → machine bearings → machine frame.

The impedance circuit model of the electric machine is shown in Fig. 2, and both path A and path B are shown in the figure.

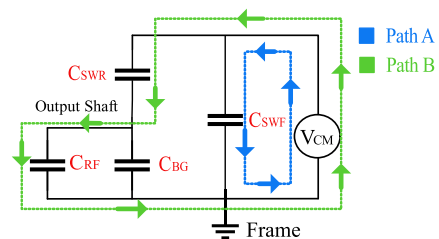


FIGURE 2. Electrical machine impedance circuit model.

In path A, the stator core is directly connected to the frame with neglectable impedance. The main impedance in this

path is the slot insulation capacitance C_{SWF} , which is the simplification of a group of capacitors instead of a simple capacitor. It includes the capacitance of the winding copper and the capacitance of the stator iron core. In this path the electrical stress is applied to the winding insulation system, leading to the aging of the insulation system.

In path B, the main impedances are the capacitance between the winding and the rotor C_{SWR} and the bearing capacitance C_{BG} . In this path, the voltage will pass through the bearings, and once the voltage is beyond the threshold, bearing current will occur. The appearance of the bearing current can damage the bearing, causing electrical erosion and impacting its lifetime [26]. An equation to describe the bearing life at the electrical side is

$$Lifetime = 7867204 \times 10^{-2.17(\frac{APK}{mm^2})} \quad (2)$$

where the lifetime in (2) is in the unit of hours, and APK is the amplitude of the bearing current [14].

III. MMC OPERATION AND CM VOLTAGE REDUCTION STRATEGY

A. MMC OPERATION PRINCIPLES

The schematic diagram of the studied MMC which is based on [27] is shown in Fig. 3. For an $n + 1$ level MMC, each arm of the MMC consists of n number of submodules and one arm inductor L_0 . The presence of the arm inductor in the circuit can prevent inrush current [5], and it can limit the circulating current as well.

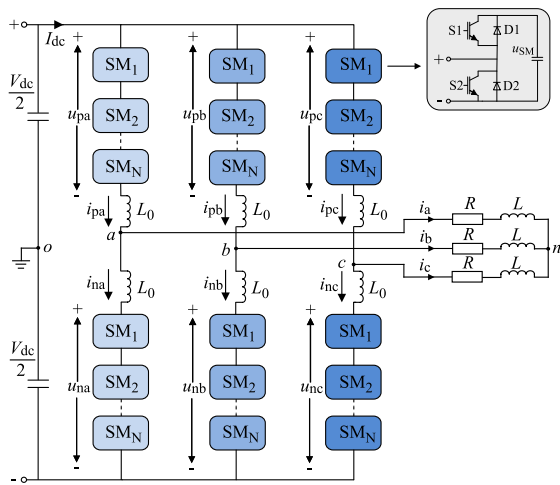


FIGURE 3. Schematic diagram of the studied MMC.

As shown Fig. 3, the studied SM is an IGBT half-bridge module. The half-bridge SM consists of two IGBT-diode switch pairs and one capacitor, and the two IGBTs in the half-bridge SM are being switched in a complementary mode. The SM can be inserted into or bypassed from the circuit, depending on the switching states of the two IGBTs and the direction of the arm current.

To achieve the normal operation of MMC, the submodule capacitors voltage needs to be controlled and balanced. The

classical sorting and balancing algorithm, which is based on the submodule capacitor voltages comparison and the polarity of the arm currents, is employed at the modulation stage in this study [28], [29].

In addition to the submodule capacitors voltage control and balancing, the circulating currents, which flow internally between the converter legs, need to be suppressed. The presence of the circulating currents can increase the conduction loss in the MMC, thus reducing the efficiency of the converter [5]. Therefore, it is important to suppress the amplitude of the circulating currents in the MMC operation. The double-line frequency circulating current controller which was introduced in [30] is used to limit the circulating currents in this study.

Various modulation techniques, such as the PWM, SVM, and NLM have been successfully used in MMC applications [25]. Among those different modulation techniques, SVM is the most interesting one due to its flexibility in the design of the switching states.

The same as in the two-level SVM, the primary task of the SVM for a multilevel converter is to find the three closest voltage vectors and their corresponding dwell time which can be used to synthesize the reference voltage vector. To tackle the challenge of a large number of redundant switching states in an MMC with a high number of SMs, a generalized SVPWM method for the multilevel converter is proposed in [31]. This method has been successfully utilized for modulating a five-level NPC converter and a five-level MMC in [32] and [33] respectively. The details of this generalized SVM method for modulating the MMC can be found in [33]. The optimal sequence of SVM for the first sector in the MMC is shown in Fig. 4 [34].

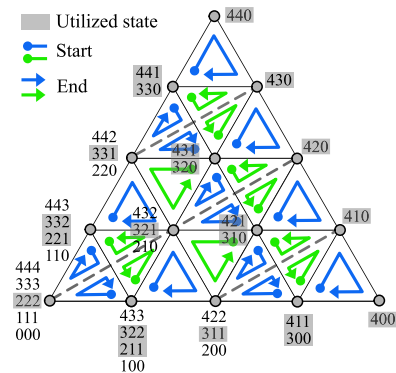


FIGURE 4. Optimal SVM sequence for a five-level MMC.

The switching states marked with grey color in Fig. 4 are utilized in the SVM, and there are two types of switching state sequences in this SVM method, the clockwise and counter-clock sequences. The clockwise sequence is marked with blue color in Fig. 4 and the counter-clock one is marked with green color. The start switching state is marked with a dot symbol while the end switching state is marked with an arrow symbol.

B. CMV REDUCTION STRATEGIES

The general expression for the CM voltage in the studied application has been shown in (1), and when observing the schematic diagram in Fig. 3, the expressions of the phase voltages can be written as

$$V_{ao} = \frac{V_{dc}}{2} - n_{p,a}E_{sm} = -\frac{V_{dc}}{2} + n_{n,a}E_{sm} \quad (3a)$$

$$V_{bo} = \frac{V_{dc}}{2} - n_{p,b}E_{sm} = -\frac{V_{dc}}{2} + n_{n,b}E_{sm} \quad (3b)$$

$$V_{co} = \frac{V_{dc}}{2} - n_{p,c}E_{sm} = -\frac{V_{dc}}{2} + n_{n,c}E_{sm} \quad (3c)$$

where $n_{p,a}$, $n_{p,b}$ and $n_{p,c}$ are the number of on-state submodules of upper arms, and $n_{n,a}$, $n_{n,b}$ and $n_{n,c}$ are the number of on-state submodules of lower arms. Inserting (3) into (1), V_{cm} can be derived as

$$\begin{aligned} V_{cm} &= \frac{V_{dc}}{2} - \frac{n_{p,a} + n_{p,b} + n_{p,c}}{3} E_{sm} \\ &= -\frac{V_{dc}}{2} + \frac{n_{n,a} + n_{n,b} + n_{n,c}}{3} E_{sm} \end{aligned} \quad (4)$$

Take a five-level MMC as an example, $V_{dc} = 4E_{sm}$, thus, (5) can be rewritten as

$$\begin{aligned} V_{cm} &= \frac{6 - (n_{p,a} + n_{p,b} + n_{p,c})}{3} E_{sm} \\ &= \frac{-6 + (n_{n,a} + n_{n,b} + n_{n,c})}{3} E_{sm} \end{aligned} \quad (5)$$

Based on (5), it can be seen that if $n_{p,a} + n_{p,b} + n_{p,c} = 6$, then $V_{cm} = 0$, if $n_{p,a} + n_{p,b} + n_{p,c} = 7$ then $V_{cm} = -\frac{1}{3}E_{sm}$, if $n_{p,a} + n_{p,b} + n_{p,c} = 5$ then $V_{cm} = \frac{1}{3}E_{sm}$. For the selected five-level MMC, the amplitude of CMV can be limited to 0 or $\frac{1}{3}E_{sm}$ with the designed number of inserted submodules in each phase. Therefore, two types of CM reduction strategies have been investigated in this study, one is the complete CMV reduction strategy, and the other one is the partial CMV reduction strategy.

1) COMPLETE CMV REDUCTION STRATEGY

Complete CMV reduction means that the CMV amplitude will be controlled to be zero with the designed switching states. As described in the previous section, to achieve the zero CMV goal in the five-level MMC, the number of the total inserted SMs in all three phases for all the switching states should be 6, and this can be achieved by selecting the switching states which are marked with magenta color in Fig. 5.

The reference voltage will be synthesized by the three closest voltage vectors in the switching states plane in Fig. 5. For instance, the reference voltage \vec{V}_{ref} can be synthesized with vectors \vec{V}_1 , \vec{V}_2 , and \vec{V}_3 in Fig. 5. If the switching state of \vec{V}_1 is [321], the switching state of \vec{V}_2 is [420], and the switching state of \vec{V}_3 is [330], based on (1), the result CMV amplitude would be zero.

By connecting all the magenta voltage vectors in Fig. 5, it can be seen that the new voltage vectors that can be used to

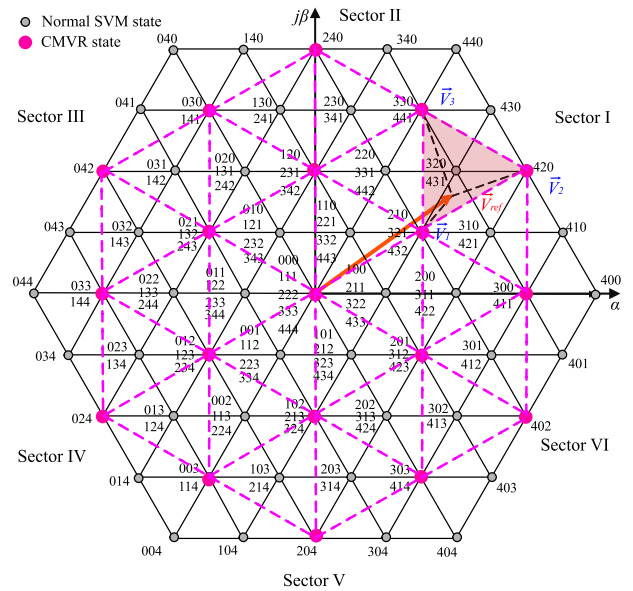


FIGURE 5. SVM-based complete CMV reduction strategy.

reduce the CM voltage construct a new space vector plane for a three-level converter. Therefore, when synthesizing \vec{V}_{ref} with the magenta voltage vectors, the first step is to utilize the aforementioned generalized SVM method to get the switching states for the “three-level” converter, then, the switching states of the five-level converter can be acquired by multiplying the “three-level” switching states with a converting matrix [24],

$$n_a = \frac{4}{2} \left(1 + \frac{1}{4-2} (n'_a - n'_b) \right) \quad (6a)$$

$$n_b = \frac{4}{2} \left(1 + \frac{1}{4-2} (n'_b - n'_c) \right) \quad (6b)$$

$$n_c = \frac{4}{2} \left(1 + \frac{1}{4-2} (n'_c - n'_a) \right) \quad (6c)$$

where n'_a , n'_b , and n'_c are the number of the inserted SMs in each phase in the “three-level” converter; and n_a , n_b and n_c are the number of the inserted SMs in each phase in the five-level converter.

2) PARTIAL CMV REDUCTION STRATEGY

The PCMVR strategy means that the CMV amplitude is not limited to zero but reduced to a certain level with this strategy. For a five-level MMC, the amplitude of the CMV is reduced to one-third of the nominal submodule capacitor voltage, and this can be achieved by using the switching states marked with magenta and yellow in Fig. 6 in the modulation stage.

Similar to the normal SVM and the CCMVR strategy, three voltage vectors are utilized to synthesize the reference voltage vector. For instance, the reference voltage \vec{V}_{ref} can be synthesized with the switching states [320], [321], and [421] in Fig. 6. This is quite close to the normal SVM,

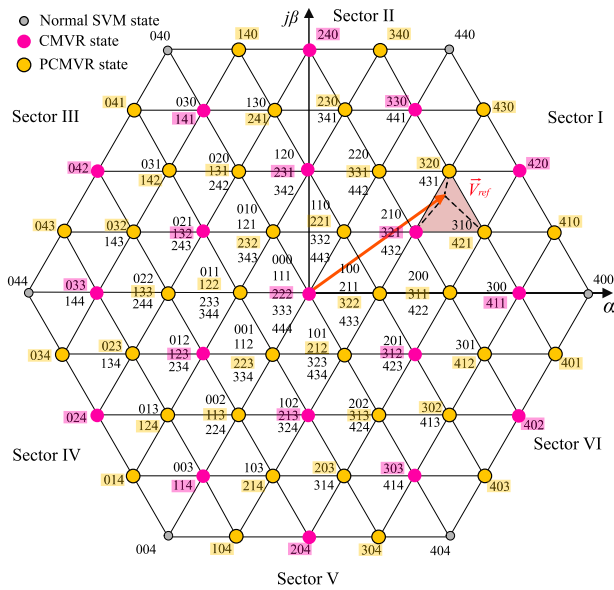


FIGURE 6. SVM-based partial CMV reduction strategy.

while the difference lies in that only three switching states are used in the PCMVR method, and this means that a five-segment switching mode is achieved in one switching period. Compared with the normal seven-segment switching mode in the normal SVM, the switching loss in the PCMVR strategy can be reduced to some extent.

The designed optimal switching states of the PCMVR strategy in this study are illustrated in Fig. 7.

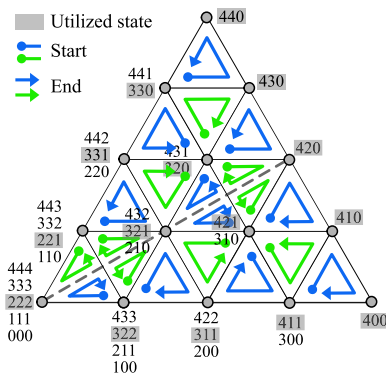


FIGURE 7. Optimal switching sequence in the designed PCMVR strategy.

The design principle in the PCMVR is to introduce the least switching events during the transition from one switching state to another, in addition to that, the switching states are designed to be symmetrically distributed, thus they can benefit the current THD. The utilized switching state is greyed in Fig. 7, and the start switching state is marked with a dot symbol while the end switching state is marked with an arrow symbol.

IV. SIMULATION RESULTS

To demonstrate the feasibility of different CMV reduction strategies, a simulation model of a five-level MMC and a three-phase *RL* load are built in MATLAB Simulink and PLECS, and the parameters of the system are listed in Table 1.

TABLE 1. The simulation MMC and *RL* load parameters.

Parameters	Value	Unit
Nominal power P	4	MW
DC-link voltage V_{dc}	12	kV
Submodules number N_{SM}	4	/
Submodule voltage E_{SM}	3	kV
Submodule capacitance C_{SM}	1.41	mF
Arm inductance L_{arm}	5	mH
Switching frequency f_{sw}	2000	Hz
Output frequency f	50	Hz
Load resistance R_{load}	15	Ω
Load inductance L_{load}	5	mH

A. WAVEFORMS OF SIMULATION RESULTS

The simulated waveforms of the three-phase currents and the CMV for the case without any CMV reduction, PCMVR strategy, and CCMVR strategy are shown in Fig. 8, Fig. 9 and Fig. 10 respectively.

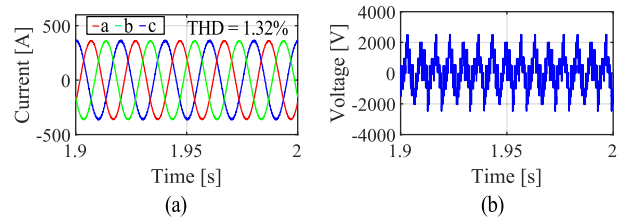


FIGURE 8. Simulated waveforms without CMV reduction strategy: (a) Three-phase currents. (b) CMV.

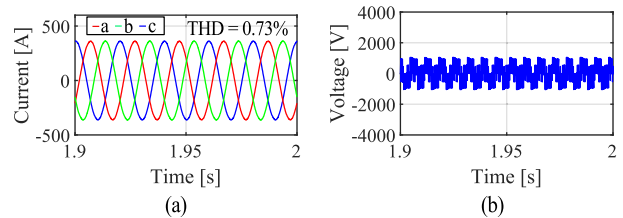


FIGURE 9. Simulated waveforms with PCMVR strategy: (a) Three-phase currents. (b) CMV.

B. ANALYSIS ON WAVEFORMS OF SIMULATION RESULTS

From the three-phase currents waveforms in Fig. 8, Fig. 9 and Fig. 10, it can be seen that the currents have sinusoidal waveforms, and the current THD are less than 5% with the given simulation parameters. In addition to the currents, the CMVs in Fig. 8, Fig. 9 and Fig. 10 indicate that the designed PCMVR and CCMVR strategies can successfully reduce the

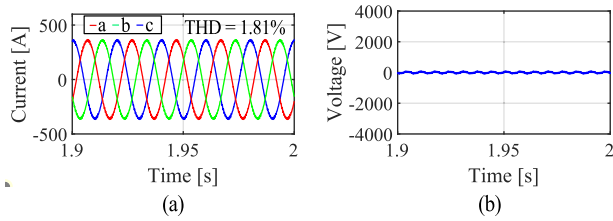


FIGURE 10. Simulated waveforms with CCMVR strategy: (a) Three-phase currents. (b) CMV.

amplitude of the CMV to the desired value. In Fig. 9b, the amplitude of the CMV is limited to 1 kV, which is one-third of the nominal value of the SM voltage E_{SM} , and this corresponds to the design of the PCMVR strategy. In Fig. 10b, the amplitude of the CMV is limited around 0 V, and this means that using the switching states in Fig. 5, the CMV can be fully eliminated.

C. ANALYSIS ON SIMULATION RESULTS OF LOSSES AND CURRENT THD

To further investigate the impact of different CMV strategies on the system, the losses of one IGBT half-bridge submodule in these cases are simulated, and the results are shown in Fig. 11. The model of the IGBT used in the simulation is ABB HiPak 5SNA0650J450300, and the blocking voltage is 6.5 kV, and this means only 1 switch is needed in each switch position in the half-bridge submodule. Moreover, the phase current THDs are presented in Fig. 11 along with the loss results.

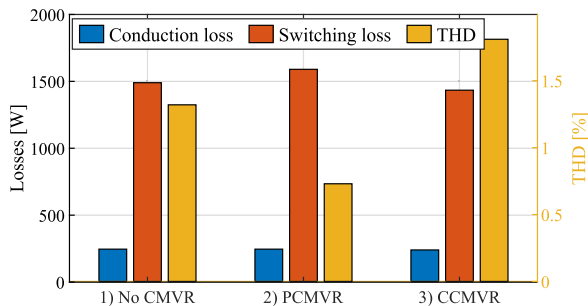


FIGURE 11. Simulation results of losses and current THD in one submodule for different CMV reduction strategies.

As shown in Table 1, the nominal power of the system is 4 MW. From Fig. 11, it can be seen that the conduction loss for all three cases is at the same level, while the switching loss differs from case to case. The switching loss of the PCMVR strategy is the highest, the switching loss of the case without CMV reduction is the second highest, and the switching loss of the CCMVR strategy is the lowest. When observing the current THD results in Fig. 11, it can be seen that the current THD of the CCMVR strategy is the highest while the current THD of the PCMVR strategy is the lowest.

The results in Fig. 11 indicate that the CCMVR strategy brings higher current THD at the system level while the total

losses are not increased compared to the case without CMV reduction. This can be justified based on the switching states plane in Fig. 5, since when changing from one switching state to another, two switching events need to be implemented in two different phases, and there is no intermediate switching state that can help with the transient, thus resulting in a higher current THD in the system. However, when counting the total number of switching events in a certain period, it can be found the number is the same for the CCMVR strategy and the case without CMV reduction, therefore, the switching loss of these two cases is at the same level. Nevertheless, a significant drawback of the CCMVR strategy is the low DC-link voltage utilization, which is limited by its mechanism.

For the results of the PCMVR strategy, it can be seen that the switching loss is the highest, and this is due to the fact the designed switching sequence in Fig. 6 results in more switching events in a certain period than the other two cases. However, the switching sequence of the PCMVR strategy only needs a five-segment SVM scheme, which is less than the normal seven-segment SVM, thus the switching loss can be reduced. Therefore, the switching loss of the designed PCMVR strategy is higher but at a similar level as the other two cases. Apart from the reduced CMV amplitude, another benefit of the designed PCMVR strategy is the reduced current THD, and this is due to a symmetrical switching sequence and more switching events.

D. CONCLUSION ON SIMULATION RESULTS

In general, the simulation results show that the designed CMVR strategies can achieve the target of limiting the CMV amplitude. At the same time, the system-level performance, such as the losses and current THD, can be affected. In the given simulation conditions, the PCMVR strategy shows a better overall performance compared with the CCMVR strategy.

V. EXPERIMENT RESULTS

A. LAB SETUP

To verify the ability of different CMV reduction strategies, experiments have been conducted in this study. The main method in the experiment is to study the impact of the CMV on the bearing current, which is based on path B of the equivalent circuit model in Fig. 2. Therefore, a lab setup is designed to measure the main bearing current when the main bearing voltage is over the threshold, and the schematic of the configuration of the lab setup is shown in Fig. 12.

In the configuration, a five-level MMC is used to drive an electric machine in a wind turbine emulator in motor mode, and the physical setup of the five-level MMC and the wind turbine emulator are shown in Fig. 13.

With the purpose of increasing the motor load, three resistors are connected to the winding in parallel. Furthermore, by this connection setup, the neutral point of the electric machine can be accessed from the resistor “Y” point instead of the stator windings. From the mechanical side, the motor

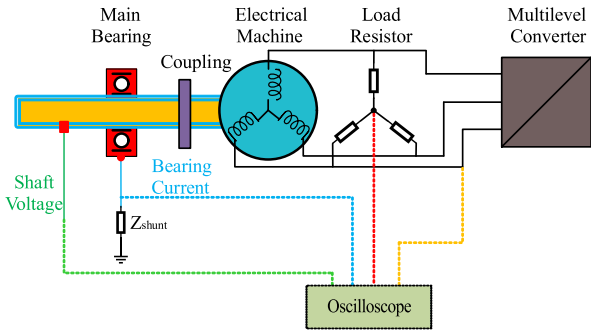


FIGURE 12. Bearing current lab test connection.

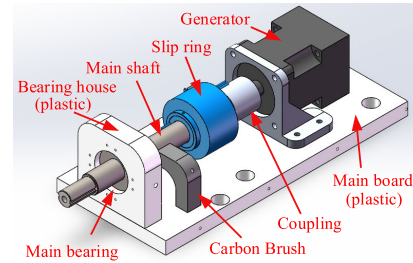


FIGURE 14. Detailed description of the wind turbine emulator.

TABLE 2. The experimental five-level MMC parameters.

Parameters	Value	Unit
DC-link voltage V_{dc}	100	V
Submodules number N_{SM}	4	/
Submodule voltage E_{SM}	25	V
Submodule capacitance C_{SM}	5	mF
Arm inductance L_{arm}	2.3	mH
Switching frequency f_{sw}	1000	Hz
Output frequency f	50	Hz
Load resistance R_{load}	15	Ω
Load inductance L_{load}	5	mH

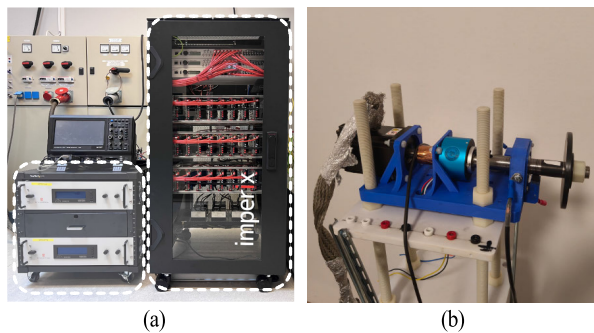


FIGURE 13. Experimental setup: (a) The DC power supply and the five-level MMC. (b) Wind turbine emulator.

shaft is connected to the main shaft of the wind turbine emulator which is supported by a separate bearing. A carbon brush is also mounted on the main shaft to monitor the shaft voltage. The separate cylinder roller bearing, which is the target test bearing, is a roller bearing with line contact between the roller and its races. Compared with the ball bearing inside the electrical machine, the roller bearing's line contact area is much larger than the ball bearing's point contact area. Thus, the capacitance of the roller bearing is larger than the ball bearing.

The details of each component in the wind turbine emulator are illustrated in Fig. 14. The target test bearing is mounted in the bearing house which is made of plastic via 3D printing technology. Its outer ring is locked inside the bearing house by a screw from the side of the bearing. From the electrical aspect view, the target bearing inner ring is connected to the electrical machine's output shaft, and its outer ring is conducted to the ground via a shunt resistor. Thus the target bearing's voltage can be measured by the carbon brush, and the bearing current can be measured via the voltage on the shunt resistor.

The parameters of the five-level MMC are listed in Table 2.

B. MEASURED WAVEFORMS OF EXPERIMENT RESULTS

The measured phase currents, CMV, main bearing voltage, and the bearing current for different cases are shown in Fig. 15, Fig. 16, and Fig. 17 respectively.

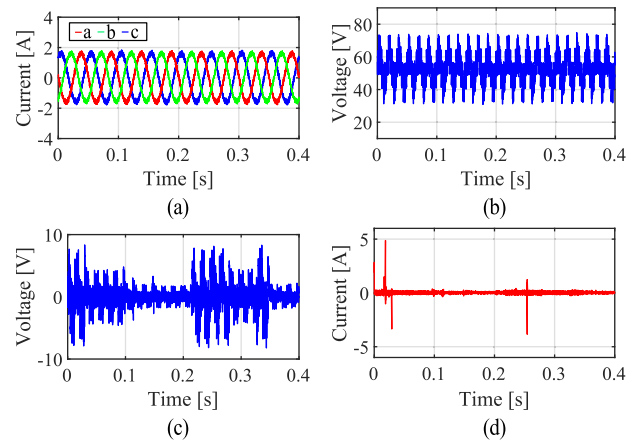


FIGURE 15. Experiment results, without CMV reduction. (a) Three-phase currents. (b) CMV. (c) Main bearing voltage. (d) Main bearing current.

C. ANALYSIS ON EXPERIMENT RESULTS

When observing the three-phase currents in the experiment results for different cases, it can be seen that for the case without CMV reduction and with the PCMVR strategy, the currents are fairly sinusoidal, while for the case with the CCMVR strategy, the currents have been strongly distorted and are not sinusoidal anymore. This means that the current THD of the CCMVR strategy is the highest compared to the other two cases, and this is in line with the simulation results. Another reason for this is that the inductance of the electric machine is quite small in the experiment setup, thus causing the currents to be less sinusoidal in the CCMVR case.

The CMVs in the experiment results are measured with respect to the negative side of the DC-link of the converter,

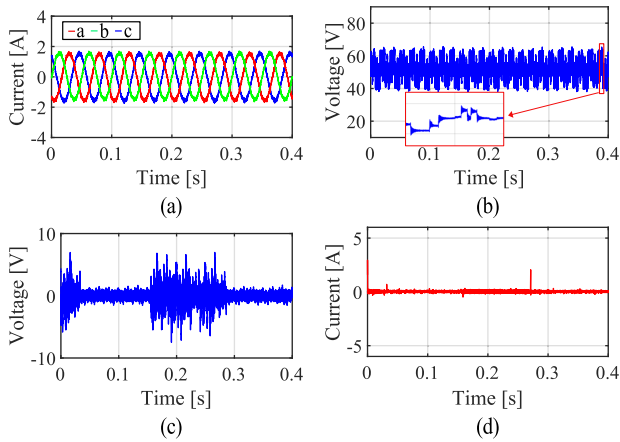


FIGURE 16. Experiment results, with PCMVR strategy. (a) Three-phase currents. (b) CMV. (c) Main bearing voltage. (d) Main bearing current.

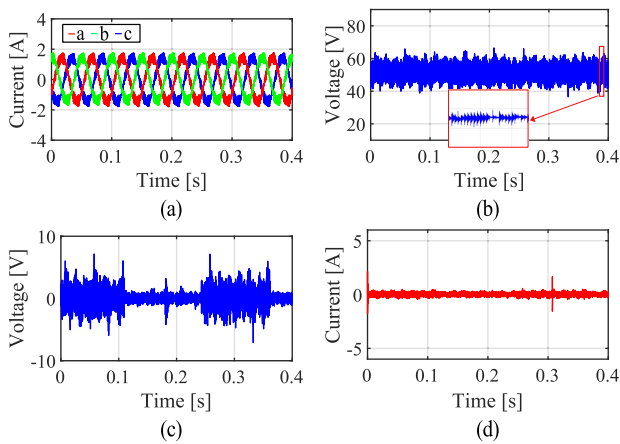


FIGURE 17. Experiment results, with CCMVR strategy. (a) Three-phase currents. (b) CMV. (c) Main bearing voltage. (d) Main bearing current.

not the middle point of it, thus the results have a DC offset of 50 V. Compared with the CMV results in the simulation for different cases, it can be seen that for the normal SVM and PCMVR cases, the CMVs show similar waveforms both in the simulation and in the experiment: the amplitude of the normal SVM case is around $\frac{2}{3}E_{sm}$; and the amplitude of the PCMVR case is around $\frac{1}{3}E_{sm}$. However, the CMV results of the simulation and the experiment for the CCMVR case are different: the CMV amplitude of the CCMVR case in the experiment is higher than the expected 0 in the simulation result. To further investigate this, a zoomed-in view of the CMV for the CCMVR case is presented in Fig. 18.

From Fig. 18, it can be seen that for the case of CCMVR, the CMV is limited to around half of the DC-link voltage which is 50 V, while there are some oscillations around the switching events, which caused that the CMV seems not to be reduced as intended. The reason for these oscillations is the stray inductance in the submodule of the MMC, and the submodules are off-the-shelf products with fixed capacitor connections, making it impossible to alternate. If we take

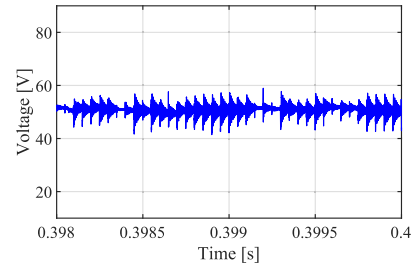


FIGURE 18. Zoomed-in view of the experimental results of CMV for the CCMVR case.

out the effect of the oscillations in the CMV in the CCMVR case, it can be seen that the CMV is limited as desired. Therefore, the physical constraints of the experiment setup led to the deviation in the CMV experiment result compared to the simulation for the CCMVR case, and this deviation could be improved with a better design and connection of the submodules in the MMC.

When observing the measured voltage and current in the main bearing in Fig. 15, Fig. 16, and Fig. 17, the conclusion is similar to the analysis of the CMVs. For the case of PCMVR, it can be seen that the amplitude of the voltage in the main bearing is reduced; the events that caused the current to be presented in the main bearing are reduced; and the bearing current amplitude is reduced as well. For the case of CCMVR, due to the oscillations of the voltage around the switching events, the voltage in the main bearing is not greatly reduced, but it is still less than the case with the PCMVR strategy. The total amount of events that caused the current to be present in the main bearing is reduced compared with normal SVM operation but it is similar to the case of PCMVR. However, when checking the bearing current amplitude of the three cases, it can be seen that the case without CMVR strategy introduces the highest current amplitude of 4.87 A, and the case using PCMVR strategy introduces a current amplitude of 2.95 A, and the case using CCMVR strategy introduces the lowest current amplitude of 1.67 A. Inserting these current amplitude values into (2), considering the hertz contact area and the bearing current occurrence frequency in all three cases, the ratio of the electrical lifetime between them is 1 : 49 : 416. Therefore, by using the CMVR strategies, the lifetime of the bearing can be greatly prolonged compared to the case without CMVR strategy, thus increasing the system's reliability.

D. CONCLUSION ON EXPERIMENT RESULTS

In general, based on the path B in the equivalent circuit model in Fig. 2, the CMV voltage does have an impact on the main bearing, and different CMV reduction strategies can help with the main bearing voltage and current amplitude. The PCMVR strategy shows the best performance in the given experiment conditions.

VI. CONCLUSION

This study investigates the common mode voltage in systems where an electric machine is driven by a converter, focusing on different SVM-based CMV reduction strategies. Both simulation and experimental analyses were conducted to evaluate the effectiveness of these strategies.

The simulation results demonstrate that both PCMVR and CCMVR strategies can effectively limit the CMV amplitude as intended. However, they exhibit different trade-offs: the PCMVR strategy results in a 6.7% increase in switching losses but achieves the lowest current THD (0.73%). Conversely, the CCMVR strategy can maintain the CMV amplitude near zero, reducing switching loss by 3.9%, but it results in the highest current THD (1.81%) and limited DC-link voltage utilization.

Experimental results with a wind turbine emulator reveal that CMV significantly impacts the main bearing. Implementing a CMV reduction strategy reduces not only the amplitude of the bearing current but also the number of the bearing current events, thus increasing the reliability of the system. Based on the bearing lifetime analysis, the PCMVR strategy extends the bearing lifetime by a factor of 49, while the CCMVR strategy extends it by a factor of 416, both relative to no CMV reduction. Among the tested strategies, PCMVR shows a better performance under the given experimental conditions, achieving the best balance between reducing CMV impact on the bearing and maintaining manageable switching loss and current THD.

However, a potential integration challenge of the studied CMVR strategies within existing power systems is the implementation complexity of CMVR strategies, due to the requirement for a predefined switching sequence. This predefined sequence reduces the flexibility of using redundant switching states for multilevel converters, such as the neutral point voltage balancing in the neutral-point-clamped converters. Future work related to this study could involve further investigation into designing switching sequences with less implementation complexity.

Overall, this study underscores the importance of selecting appropriate CMV reduction strategies to mitigate bearing-related failures in wind turbine applications and potentially other electric drive systems.

REFERENCES

- [1] P. C. Sen, "Electric motor drives and control—past, present, and future," *IEEE Trans. Ind. Electron.*, vol. 37, no. 6, pp. 562–575, Jul. 1990.
- [2] H. Abu-Rub, J. Holtz, J. Rodriguez, and G. Baoming, "Medium-voltage multilevel converters—State of the art, challenges, and requirements in industrial applications," *IEEE Trans. Ind. Electron.*, vol. 57, no. 8, pp. 2581–2596, Aug. 2010.
- [3] S. Kouro, J. Rodriguez, B. Wu, S. Bernet, and M. Perez, "Powering the future of industry: high-power adjustable speed drive topologies," *IEEE Ind. Appl. Mag.*, vol. 18, no. 4, pp. 26–39, Jul. 2012.
- [4] H. Abu-Rub, S. Bayhan, S. Moinoddin, M. Malinowski, and J. Guzinski, "Medium-voltage drives: Challenges and existing technology," *IEEE Power Electron. Mag.*, vol. 3, no. 2, pp. 29–41, Jun. 2016.
- [5] B. Wu and M. Narimani, *High-Power Converters and AC Drives* (IEEE Press Series on Power Engineering), 2nd ed., Hoboken, NJ, USA: IEEE Press, 2017.
- [6] M. Kriese, E. Wittek, S. Gattermann, H. Tischmacher, G. Poll, and B. Ponick, "Influence of bearing currents on the bearing lifetime for converter driven machines," in *Proc. XXth Int. Conf. Electr. Mach.*, Sep. 2012, pp. 1735–1739.
- [7] M. Riera-Guasp, J. A. Antonino-Daviu, and G.-A. Capolino, "Advances in electrical machine, power electronic, and drive condition monitoring and fault detection: State of the art," *IEEE Trans. Ind. Electron.*, vol. 62, no. 3, pp. 1746–1759, Mar. 2015.
- [8] T. Plazenet, T. Boileau, C. Caironi, and B. Nahid-Mobarakkeh, "A comprehensive study on shaft voltages and bearing currents in rotating machines," *IEEE Trans. Ind. Appl.*, vol. 54, no. 4, pp. 3749–3759, Jul. 2018.
- [9] X. Gong and W. Qiao, "Bearing fault diagnosis for direct-drive wind turbines via current-demodulated signals," *IEEE Trans. Ind. Electron.*, vol. 60, no. 8, pp. 3419–3428, Aug. 2013.
- [10] M. Whittle, "Wind turbine generator reliability: an exploration of the root causes of generator bearing failures," Ph.D. dissertation, School Eng. Comput. Sci., Durham Univ., Durham, U.K., 2013.
- [11] R. Liu, X. Ma, X. Ren, J. Cao, and S. Niu, "Comparative analysis of bearing current in wind turbine generators," *Energies*, vol. 11, no. 5, p. 1305, May 2018.
- [12] S. Chen, T. A. Lipo, and D. Fitzgerald, "Source of induction motor bearing currents caused by PWM inverters," *IEEE Trans. Energy Convers.*, vol. 11, no. 1, pp. 25–32, Mar. 1996.
- [13] J. M. Erdman, R. J. Kerkman, D. W. Schlegel, and G. L. Skibinski, "Effect of PWM inverters on AC motor bearing currents and shaft voltages," *IEEE Trans. Ind. Appl.*, vol. 32, no. 2, pp. 250–259, Aug. 1996.
- [14] D. Busse, J. Erdman, R. J. Kerkman, D. Schlegel, and G. Skibinski, "Bearing currents and their relationship to PWM drives," *IEEE Trans. Power Electron.*, vol. 12, no. 2, pp. 243–252, Mar. 1997.
- [15] A. Muetze, *Bearing Currents in Inverter-Fed AC-Motors*. Düren, Germany: Shaker-Verlag, 2004.
- [16] Y. Gemeinder and M. Weicker, "Application guide bearing currents," Institut für Elektrische Energiewandlung, Technische Universität Darmstadt, Darmstadt, Germany, 2021.
- [17] O. Magdun, Y. Gemeinder, A. Binder, and K. Reis, "Calculation of bearing and common-mode voltages for the prediction of bearing failures caused by EDM currents," in *Proc. 8th IEEE Symp. Diag. Electr. Mach., Power Electron. Drives*, Sep. 2011, pp. 462–467.
- [18] O. Magdun and A. Binder, "Calculation of roller and ball bearing capacitances and prediction of EDM currents," in *Proc. 35th Annu. Conf. IEEE Ind. Electron.*, Nov. 2009, pp. 1051–1056.
- [19] W. Zhai, L. Shi, and Z. Y. Sun, "Study on passive filter in wind power converter," in *Proc. IEEE Int. Conf. Appl. Supercond. Electromagn. Devices*, Oct. 2013, pp. 229–232.
- [20] A. Joshi and J. Blennow, "Electrical characterization of bearing lubricants," in *Proc. IEEE Conf. Electr. Insul. Dielectric Phenomena (CEIDP)*, Oct. 2014, pp. 586–589.
- [21] L. Jia, R. Liu, Z. Li, S. Li, and X. Huang, "Modelling and suppression of bearing voltage of wind turbine permanent magnet synchronous generators," *IET Electric Power Appl.*, vol. 18, no. 4, pp. 436–445, Apr. 2024. [Online]. Available: <https://ietresearch.onlinelibrary.wiley.com/doi/abs/10.1049/elp2.12403>
- [22] F. Wang, A. K. Wallace, S. Dai, A. Von Jouanne, and H. Zhang, "Multilevel inverter modulation schemes to eliminate common-mode voltages," *IEEE Trans. Ind. Appl.*, vol. 36, no. 6, pp. 1645–1653, Jul. 2000.
- [23] A. Edpuganti and A. K. Rathore, "Optimal pulsewidth modulation for common-mode voltage elimination scheme of medium-voltage modular multilevel converter-fed open-end stator winding induction motor drives," *IEEE Trans. Ind. Electron.*, vol. 64, no. 1, pp. 848–856, Jan. 2017.
- [24] C.-H. Park, I.-K. Seo, B. B. Negesse, J.-S. Yoon, and J.-M. Kim, "A study on common mode voltage reduction strategies according to modulation methods in modular multilevel converter," *Energies*, vol. 14, no. 6, p. 1607, Mar. 2021. [Online]. Available: <https://www.mdpi.com/1996-1073/14/6/1607>
- [25] S. Debnath, J. Qin, B. Bahrani, M. Saeedifard, and P. Barbosa, "Operation, control, and applications of the modular multilevel converter: A review," *IEEE Trans. Power Electron.*, vol. 30, no. 1, pp. 37–53, Jan. 2015.
- [26] Z. Jian, "On wind turbine main shaft bearing currents," Licentiate thesis, Chalmers Univ. Technol., Gothenburg, Sweden, 2024.
- [27] J. Rodriguez, J.-S. Lai, and F. Zheng Peng, "Multilevel inverters: A survey of topologies, controls, and applications," *IEEE Trans. Ind. Electron.*, vol. 49, no. 4, pp. 724–738, Aug. 2002.

- [28] S. Rohner, S. Bernet, M. Hiller, and R. Sommer, "Modulation, losses, and semiconductor requirements of modular multilevel converters," *IEEE Trans. Ind. Electron.*, vol. 57, no. 8, pp. 2633–2642, Aug. 2010.
- [29] E. Solas, G. Abad, J. A. Barrena, S. Aurtenetxea, A. Cárcar, and L. Zajac, "Modular multilevel converter with different submodule concepts—Part I: Capacitor voltage balancing method," *IEEE Trans. Ind. Electron.*, vol. 60, no. 10, pp. 4525–4535, Oct. 2013.
- [30] Q. Tu, Z. Xu, and L. Xu, "Reduced switching-frequency modulation and circulating current suppression for modular multilevel converters," *IEEE Trans. Power Del.*, vol. 26, no. 3, pp. 2009–2017, Jul. 2011.
- [31] S. Wei, B. Wu, F. Li, and C. Liu, "A general space vector PWM control algorithm for multilevel inverters," in *Proc. 18th Annu. IEEE Appl. Power Electron. Conf. Exposit.*, vol. 1, 2003, pp. 562–568.
- [32] G. Mademlis, "Medium voltage generation system with five-level NPC converters for kite tidal power," Licentiate thesis, Chalmers Univ. Technol., Gothenburg, Sweden, 2019.
- [33] C. Tang and T. Thiringer, "Modular multilevel converter control with using a general space vector PWM method in medium voltage hydro power application," in *Proc. 24th Eur. Conf. Power Electron. Appl. (EPE ECCE Europe)*, Sep. 2022, pp. 1–11.
- [34] B. P. McGrath, D. G. Holmes, and T. Lipo, "Optimized space vector switching sequences for multilevel inverters," *IEEE Trans. Power Electron.*, vol. 18, no. 6, pp. 1293–1301, Nov. 2003.



CHENGJUN TANG (Graduate Student Member, IEEE) received the B.Sc. degree from the Department of Engineering Physics, Tsinghua University, Beijing, China, in 2011, and the M.Sc. degree in electrical power engineering from the Chalmers University of Technology, Gothenburg, Sweden, in 2018, where is currently pursuing the Ph.D. degree in electric power engineering. His research interests include power electronics area, especially in the modelling and control of multilevel converters which are used in high power and medium voltage applications.



JIAN ZHAO received the master's degree in electrical engineering from Harbin Institute of Technology, Harbin, China, in 2013. He is currently pursuing the Ph.D. degree in electric power engineering with the Chalmers University of Technology, Gothenburg, Sweden. His research interests include bearing currents in wind turbines and electrical machines, and electrical machine design in applications of renewable energy systems and electric vehicles.



TORBJÖRN THIRINGER (Senior Member, IEEE) received the M.Sc. and Ph.D. degrees in electro technology from the Chalmers University of Technology, Gothenburg, Sweden, in 1989 and 1996, respectively. He is currently working as a Professor of applied power electronics with the Chalmers University of Technology. His research interests include the modeling, control, and grid integration of wind energy converters into power grids, battery technology from detailed cell modeling to system aspects, and power electronics and drives for other types of applications, such as electrified vehicles, buildings, and industrial applications.

• • •